The role of ions in the self-healing behavior of soft particle suspensions

Andrea Scotti[a,b], Urs Gasser[a,1], Emily S. Herman[c], Miguel Pelaez-Fernandez[b], Jun Han[d,e], Andreas Menzel[d], L. Andrew Lyon[f], and Alberto Fernández-Nieves[b]

[a]Laboratory for Neutron Scattering and Imaging, Paul Scherrer Institut, 5232 Villigen, Switzerland; [b]School of Physics, Georgia Institute of Technology, Atlanta, GA 30332; [c]School of Chemistry and Biochemistry, Georgia Institute of Technology, Atlanta, GA 30332; [d]Laboratory for Macromolecules and Bioimaging, Paul Scherrer Institut, 5232 Villigen, Switzerland, [e]Quanzhou Institute of Equipment Manufacturing, Haixi Institutes, Chinese Academy of Sciences, Quanzhou 362200, People's Republic of China; and [f]Schmid College of Science and Technology, Chapman University, Orange, CA 92866

Edited by David A. Weitz, Harvard University, Cambridge, MA, and approved March 30, 2016 (received for review August 15, 2015)

Impurities in crystals generally cause point defects and can even suppress crystallization. This general rule, however, does not apply to colloidal crystals formed by soft microgel particles [Iyer ASJ, Lyon LA (2009) *Angew Chem Int Ed* 48:4562–4566], as, in this case, the larger particles are able to shrink and join the crystal formed by a majority of smaller particles. Using small-angle X-ray scattering, we find the limit in large-particle concentration for this spontaneous deswelling to persist. We rationalize our data in the context of those counterions that are bound to the microgel particles as a result of the electrostatic attraction exerted by the fixed charges residing on the particle periphery. These bound counterions do not contribute to the suspension osmotic pressure in dilute conditions, as they can be seen as internal degrees of freedom associated with each microgel particle. In contrast, at sufficiently high particle concentrations, the counterion cloud of each particle overlaps with that of its neighbors, allowing these ions to freely explore the space outside the particles. We confirm this scenario by directly measuring the osmotic pressure of the suspension. Because these counterions are then no longer bound, they create an osmotic pressure difference between the inside and outside of the microgels, which, if larger than the microgel bulk modulus, can cause deswelling, explaining why large, soft microgel particles feel the squeeze when suspended with a majority of smaller particles. We perform small-angle neutron scattering measurements to further confirm this remarkable behavior.

microgels | deswelling | crystallization | SAXS | SANS

Point defects in crystalline materials disrupt the crystal structure and often prevent crystallization. This is the case, for instance, when large particles are introduced in a crystal of smaller particles. Bragg illustrated the consequences of this disruption using soap bubbles (1). In metal melts, a size mismatch of 15% between the atoms suppresses crystallization (2), and, in hard spheres, which constitute an important model system for condensed matter, a polydispersity above 12% also prevents crystallization (3). Furthermore, the polydispersity in hard sphere crystals does not exceed 5.7%, due to local segregation of dissimilar particles during crystallization (4, 5).

Remarkably, these restrictions do not necessarily apply to suspensions of soft microgels, which are cross-linked polymer particles immersed in a solvent that can exist in either swollen or deswollen states, depending on external conditions like temperature (6) and pH (7). Indeed, microgel suspensions containing a small fraction of larger particles can crystallize without defects by shrinking the larger particles to a size that is identical to that of the smaller and more abundant microgel particles (8). This deswelling was hypothesized to result either from the direct interaction between large and small particles or from the osmotic pressure exerted by the small microgels on the larger ones (2). Here, we show that none of these effects drive this process. Instead, we find that the counterions bound to the microgel periphery as a result of their electrostatic attraction to the peripheral microgel charges can, at sufficiently large concentration of the small microgels, delocalize and explore the available volume outside the particles, hence exerting the required osmotic pressure to cause deswelling of the larger microgels. Interestingly, this same mechanism could also explain similar deswelling behavior in suspensions of DNA-coated colloids with star-shape architecture (9).

We use large and small temperature-responsive poly(*N*-isopropylacrylamide) (pNIPAM) microgels (10) and study aqueous suspensions with the particles in the fully swollen state at 18 °C < T < 21 °C (11). In these conditions, the radii of the large and small particles are $R_b \approx 180$ nm and either $R_s \approx 135$ nm or $R_s \approx 120$ nm, respectively, as determined by small-angle neutron scattering (SANS); see Table S1 for a detailed list of the different particles we use. These are all synthesized according to the same protocol. Furthermore, at fixed temperature, the suspension phase behavior is essentially determined by the suspension volume fraction, ϕ. However, due to microgel deformability and compressibility, the particle volume and, therefore, ϕ are difficult to quantify, particularly at high particle number densities. As a result, we use a generalized volume fraction, ζ, obtained from the polymer mass fraction and a mapping of the dilute suspension viscosity to the hard sphere expectation (*Supporting Information* and ref. 12). For low ϕ, $\zeta = \phi$. In contrast, for sufficiently high ϕ, the particles must deform and shrink to fit into the available space. As a result, ζ can take values larger than 1 at sufficiently high concentrations, whereas ϕ is, at most, equal to 1. Note that ζ is always proportional to the particle number concentration.

To study the effect of larger pNIPAM particles on the phase behavior of a suspension of smaller pNIPAM particles, we

Significance

Understanding when a material crystallizes is of fundamental importance in condensed matter. In many materials, the presence of point defects suppresses crystallization. Surprisingly, colloidal hydrogels can overcome this limitation: A small number of large microgels can spontaneously deswell to fit in the crystal lattice of smaller microgels, thus avoiding the occurrence of point defects. We find that this unique particle deswelling is due to an osmotic pressure difference between the inside and the outside of the microgels resulting from the overlap of counterion clouds of neighboring particles. When this pressure difference exceeds the bulk modulus of the large microgels, these shrink, enabling crystallization without point defects.

Author contributions: U.G. and A.F.-N. designed research; A.S. and U.G. performed research; E.S.H., M.P.-F., J.H., A.M., and L.A.L. contributed new reagents/analytic tools; A.S., U.G., and A.F.-N. analyzed data; A.S., U.G., and A.F.-N. wrote the paper; and J.H. and A.M. operated the SAXS beamline.

The authors declare no conflict of interest.

This article is a PNAS Direct Submission.

[1]To whom correspondence should be addressed. Email: urs.gasser@psi.ch.

This article contains supporting information online at www.pnas.org/lookup/suppl/doi:10.1073/pnas.1516011113/-/DCSupplemental.

prepare bidisperse suspensions at various number fractions of the large particles, n_b, which we calculate from the single-particle masses of both small and large particles and the corresponding total masses in the bidisperse sample. The total ζ of the suspension is obtained as $\zeta = \zeta_s + \zeta_b$, where ζ_s and ζ_b are calculated from the swollen volumes of the small and large particles, respectively, and the total volume of the suspension (*Supporting Information*). The small and large pNIPAM species have a polydispersity $\leq 12\%$ and crystallize at $\zeta_f \approx 0.59$, consistent with previous experiments with the same type of particles (12).

For each n_b, a series of suspensions is prepared covering a ζ-range containing both the freezing and melting points of the suspension of small microgels; typically $0.5 \lesssim \zeta \lesssim 0.9$. The size ratio of the small and large particles is within the range $0.74 < R_s/R_b < 0.78$ for all sample series (*Supporting Information*). We use small-angle X-ray scattering (SAXS) to characterize the phase behavior and elucidate the response of the large particles. We obtain the structure factor, $S(q)$, by dividing the measured scattered intensity, $I(q)$, by the form factor, $P(q)$ (*Supporting Information* and refs. 11 and 13), which we independently determine with dilute samples. An example of a detector image and the corresponding $S(q)$ is shown in Fig. 1*A* for a bidisperse sample in the glassy state with $n_b = (1.4 \pm 0.1)\%$ and $\zeta = 0.76 \pm 0.02$. In this case, we use the position of the first peak in $S(q)$ to obtain the nearest neighbor distance, d_{nn}; we do the same for all liquid and glassy samples. However, for crystalline samples, we find that $S(q)$ is consistent with a random hexagonal close packed structure for both monodisperse and bidisperse samples; this structure is consistent with what has been reported before for similar and other microgel suspensions and is also realized by hard and charged spheres (14–18). In this case, we obtain the lattice constant and hence d_{nn} from the position of the second ring of Bragg peaks, which can be clearly seen in the detector image, as shown in Fig. 1*B* for $n_b = (6.6 \pm 0.7)\%$ and $\zeta = 0.67 \pm 0.01$. The second ring of peaks is chosen, as these peaks are true Bragg peaks, whereas the first and third rings are due to Bragg rods (19). The $d_{nn}(\zeta)$ curves for monodisperse suspensions of only small or large particles clearly reflect the size difference between the two types of particles, as shown in Fig. 1*C*.

Remarkably, we find d_{nn} in samples with $n_b = (2.3 \pm 0.2)\%$ to be the same as in monodisperse samples of only small particles, as shown by the squares in Fig. 1*D*. The decrease of d_{nn} with ζ reflects isotropic shrinkage of this length scale. Indeed, the data for the small-only and large-only suspensions, as well as that for bidisperse suspensions, follow the functional form expected in this situation: $d_{nn} = a\zeta^{-1/3}$, with a the nearest neighbor distance at $\zeta = 1$, which we use as a fitting parameter; this is shown by the curves in Fig. 1 *C* and *D*. Note that the curves for the bidisperse sample and the sample comprising only small particles virtually coincide throughout the studied ζ-range. Furthermore, for $n_b = (6.6 \pm 0.7)\%$, the Bragg peaks of the crystalline bidisperse sample, shown with squares in Fig. 1*B*, appear at the same q values as the Bragg peaks found in the monodisperse sample of only small particles, shown with circles in Fig. 1*B*. In the bidisperse sample, the absence of Bragg peaks or a fluid peak reminiscent of a crystal or fluid formed by large particles excludes segregation of small and large particles in these samples. We thus conclude that the large particles deswell and do not significantly disrupt the lattice in crystalline samples, consistent with earlier real-space observations of similar microgel suspensions (8), nor do they disrupt the small-particle arrangement in liquid and glassy samples. Note that, in our experiments, the fraction of large particles is significantly larger than that in prior experiments (8).

We directly confirm the deswelling of the large particles with SANS using contrast matching to suppress the scattering signal from the small particles (Fig. S1, *Supporting Information*, and refs. 20 and 21). We thus use deuterated small particles with $R_s = (117 \pm 7)$ nm and large particles with $R_b = (176 \pm 4)$ nm; the resulting size ratio is $R_s/R_b = 0.66 \pm 0.05$. In this situation, we directly measure the form factor of the large particles, which we fit with a well accepted core–shell model for pNIPAM microgels to obtain the particle radius (*Supporting Information*, Table S2, and refs. 11 and 13). The result for a bidisperse suspension at $\zeta = 0.85 \pm 0.05$ and $n_b = (2.9 \pm 0.3)\%$ is shown by the triangles in Fig. 2*A*. For comparison, we show with pluses in the same figure the result for a suspension of only large microgels at $\zeta \approx 0.08$, which is dilute enough to directly measure the particle form factor without contrast matching. The corresponding curve shows a faster decay with q, indicating a larger particle size in this case compared with the bidisperse situation. This confirms that the larger microgels have indeed shrunken in the bidisperse suspension. We quantify this behavior in terms of ζ and find that the radius of the larger microgels remains approximately

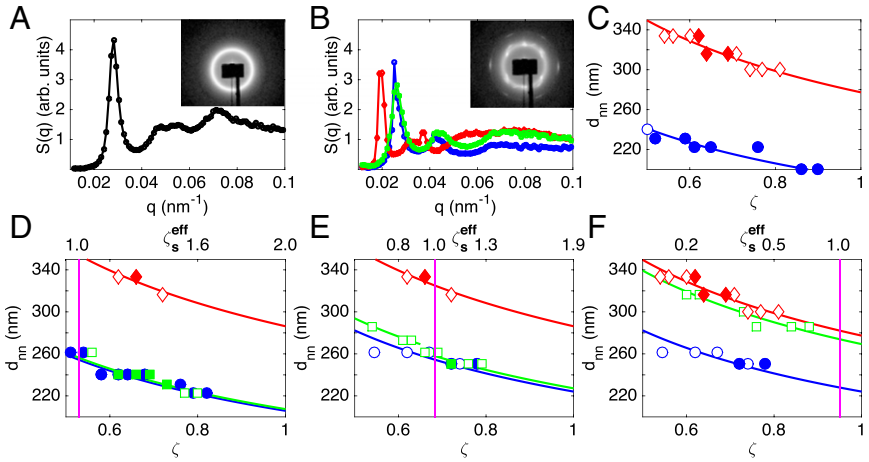

Fig. 1. (*A*) Structure factor, $S(q)$, of a glassy suspension with $n_b = (1.4 \pm 0.1)\%$ and $\zeta = 0.76 \pm 0.02$. (*Inset*) The detector image. (*B*) $S(q)$ of a bidisperse and the two corresponding monodisperse crystalline samples with (green) $n_b = (6.6 \pm 0.7)\%$ and $\zeta = 0.67 \pm 0.01$, (blue) $\zeta = 0.62 \pm 0.01$, and (red) $\zeta = 0.63 \pm 0.02$. (*Inset*) The detector image of the bidisperse sample. (*C–F*) Nearest neighbor distance, d_{nn}, versus generalized volume fraction, ζ, for (blue circles) small-only, (red diamonds) large-only, and (green squares) bidisperse suspensions with (*D*) $n_b = (2.3 \pm 0.2)\%$, (*E*) $n_b = (29 \pm 3)\%$, and (*F*) $n_b = (79 \pm 8)\%$. Crystalline samples are represented by filled symbols. The lines are fits to $d_{nn}(\zeta) = a\zeta^{-1/3}$, with a as a fitting parameter. In *D–F*, ζ_s^{eff} is given by the upper x axis, and the violet vertical line indicates a value of $\zeta_s^{eff} = 1$. The swollen radii of the particles used in all shown measurements are listed in Table S1.

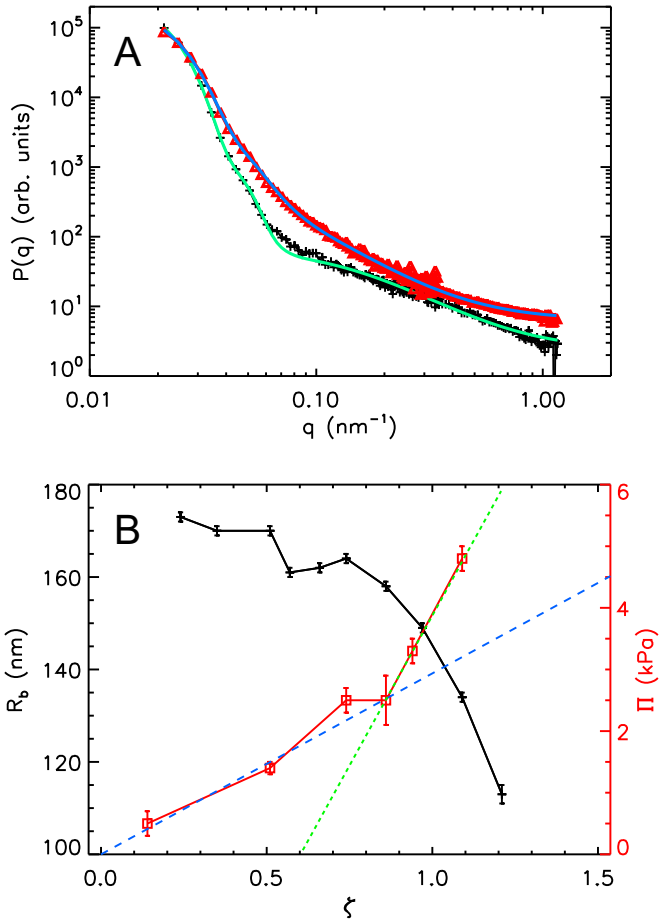

Fig. 2. (*A*) SANS form factors of the large microgels and corresponding fits in (red triangles) a bidisperse sample with $n_b = (2.9 \pm 0.3)\%$ and $\zeta = 0.85 \pm 0.05$ and in (black plus signs) a monodisperse large-only sample with $\zeta \approx 0.08$. See Table S1 for fully swollen particle radii. The lines show the form factor fits to the data. (*B*) SANS radius of the large particles (black plus signs) in the bidisperse sample shown in *A* and the osmotic pressure (red squares) vs. ζ. The dashed lines are linear fits to $\Pi(\zeta)$ for (blue) $\zeta < 0.85$ and (green) $\zeta > 0.85$ highlighting the change in slope at $\zeta \approx 0.85$.

constant and equal to the dilute radius up to $\zeta \approx 0.5$, where it decreases slightly before a more pronounced decrease at $\zeta \approx 0.85$, as shown in Fig. 2*B*. Note that $R_b = (113 \pm 2)$ nm at $\zeta \approx 1.2$, which coincides with the radius of the small microgels, $R_s = (117 \pm 7)$ nm, measured in dilute conditions and without contrast matching techniques.

Interestingly, for bidisperse suspensions with a higher $n_b = (29 \pm 3)\%$, we find that the $d_{nn}(\zeta) \propto \zeta^{-1/3}$ behavior only coincides with the corresponding behavior of suspensions with only small particles for $\zeta \gtrsim 0.67$. Below this ζ, the fits of this functional form to the data do not lie on top of each other, as shown in Fig. 1*E*. This suggests that the large particles only deswell to a size close to that of the small particles for $\zeta \lesssim 0.67$.

To explain the observed deswelling of the large particles and its dependence on n_b, we recall that, despite the fact that NIPAM is not charged, pNIPAM particles contain charged groups at their periphery resulting from the initiator, ammonium persulfate, used in the synthesis (22). As a result, our particles contain SO_3^- groups in their outskirts. Correspondingly, there are NH_4^+ counterions in solution. Interestingly, for the case of ionic microgels, which are charged throughout their bulk, these counterions control the compression of the particles (23). In this case, there is a Donnan potential inside the microgels that confines most of these counterions to the microgel interior. Only those attracted with a strength $\leq k_BT$ can leave the particles and contribute to the external osmotic pressure to potentially deswell the particles. In our case, however, most of the charge is located in the periphery of the particles rather than throughout their bulk. Hence there is a cloud of bound counterions in the peripheral region of each microgel, as shown schematically in Fig. 3*A*. In this case and in contrast to the ionic microgel case, those ions that are attracted to the peripheric charged region with a strength $\leq k_BT$, distribute both outside and inside the particles, as shown schematically in Fig. 3*A*. Hence the distribution of these unbound counterions will not result in the osmotic pressure difference between the inside and the outside of the microgel required to explain the deswelling we observe experimentally.

To confirm this, we study suspensions of particles with fully swollen radius $R = (125 \pm 5)$ nm at $\zeta \lesssim 0.08$ with added salt. Because we expect the salt ions to distribute both inside and outside of the microgels, they should not induce particle deswelling. We determine the suspension form factor using SANS at concentrations of the salt NaSCN equal to 2.5 mM, 7.1 mM, and 115.3 mM; we then fit the data with the core–shell form factor model and determine the particle radius (*Supporting Information*). We note that, at the highest salt concentration, the number of salt ions exceeds the number of counterions in our samples. We find that the form factors are virtually identical and are identical to the salt-free case, as shown with black plus signs and red triangles in Fig. 4. Consistent with this, we find $R = (125 \pm 5)$ nm for the case without added salt, and $R = (123 \pm 3)$ nm for the case with the highest salt concentration. These results thus confirm that, indeed, all unbound ions distribute themselves inside and outside the microgels without inducing a significant osmotic pressure difference.

With increasing ζ, however, the distance between particles decreases and, eventually, the clouds of those counterions that are bound to the peripheral charged region with a strength $> k_BT$ overlap. In this concentrated case, the clouds can fill the space between the particles, and these bound counterions can no longer be related to an individual microgel particle, but they rather explore the outside space, thus creating an external osmotic pressure, as schematically shown in Fig. 3*B*. This external pressure cannot be balanced by the unbound counterions inside the particles, as the counterion density inside remains essentially unchanged. We then hypothesize that the resulting osmotic pressure due to these initially bound and now delocalized counterions is the cause for the deswelling behavior of the large microgels observed experimentally.

To test this, we measure the osmotic pressure, Π, of the bidisperse suspension used in the SANS experiments using a membrane osmometer (Wescor 4420). We find that, at low ζ, Π is much larger than what is expected for a fluid of microgels. Furthermore,

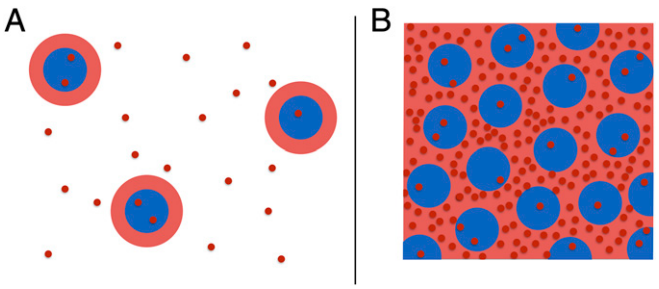

Fig. 3. Schematics of the microgel particles (blue), their counterion cloud (red rings), and free counterions (red points) (*A*) in dilute conditions and (*B*) at high concentration with percolated counterion clouds and bound counterions contributing to the osmotic pressure of the suspension.

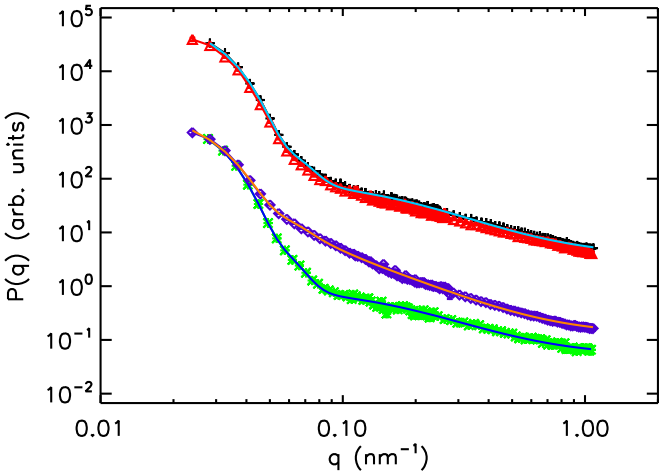

Fig. 4. SANS form factors and corresponding fits; green asterisks, monodisperse small-only sample at $\zeta \approx 0.08$; purple diamonds, bidisperse sample with $n_b = (84 \pm 3)\%$, $\zeta = 1.20 \pm 0.01$, and a radius $R = (95 \pm 5)$ nm of the deswollen small particles; black plus signs, monodisperse sample at $\zeta \approx 0.08$ with 115.3 mM NaSCN; and red triangles, same as black plus signs but without NaSCN salt. See Table S1 for fully swollen particle radii. The fit for the black plus signs is not shown.

it increases linearly with ζ up to $\zeta \approx 0.85$, as shown in Fig. 2*B* with squares. Above this ζ-value and up to the highest ζ we experimentally probe, the behavior of Π is also consistent with a linear growth. However, in this ζ-range, the slope is considerably larger than that at lower ζ, as also shown in Fig. 2*B*. The observed behavior for $\zeta \lesssim 0.85$ can be understood by realizing that Π is determined by the unbound counterions, as these are much more numerous than the microgel particles (23). Because these ions are only those that can escape the electrostatic attraction to the microgel periphery, their number must be significantly lower than the total number of counterions. By assuming an ideal gas of free counterions, we expect $\Pi = N_{free} k_B T \zeta / V_p$, with N_{free} the number of unbound counterions per particle and V_p the volume of a fully swollen microgel particle. We then fit the experimental Π versus ζ, for $\zeta \lesssim 0.85$, and obtain $N_{free} = (8 \pm 2) \cdot 10^3$ from the slope of the fit. This corresponds to a counterion density of $(9.4 \pm 2.6) \cdot 10^{-4}$ nm^{-3} at $\zeta = 0.85$, which supports the ideal gas approximation. Furthermore, from the synthesis, we estimate a total number of $N = (6.8 \pm 0.3) \cdot 10^4$ counterions per particle (*Supporting Information*). As a result, $N_{free}/N \approx 11\%$, which is small, consistent with our expectation. For larger ζ, when the clouds of bound counterions overlap, these ions would then contribute to Π. We interpret the higher slope of $\Pi(\zeta)$ for $\zeta \gtrsim 0.85$ as an indication of this fact.

The osmotic pressure behavior is thus supportive of the role played by the bound counterions in our experiments. To further confirm this, we recall that the onset of deswelling in the bidisperse suspension with $n_b = (29 \pm 3)\%$ occurs at $\zeta \approx 0.67$, highlighted by the vertical line in Fig. 1*E*, which is close to where Π appreciably changes slope. Indeed, for $\zeta \approx 0.67$, the osmotic pressure difference between the inside and outside of the particles, due to the initially bound counterions, is enough to deswell the fuzzy shell of the particles, as shown in Fig. S2*A*. As ζ progressively increases, this osmotic pressure difference increases and, eventually, also, the core of the particles gets compressed; this happens at $\zeta \approx 0.85$, as shown in Fig. S2*B*. Therefore, the change in behavior of the suspension osmotic pressure approximately occurs when the microgel particle appreciably compresses, supporting our interpretation of the results.

To further test the proposed mechanism, consider an effective particle consisting of a microgel with radius R and a cloud of bound counterions of thickness Δr; the overall particle radius is $R^{eff} = R + \Delta r$. We also introduce an effective volume fraction for the small particles in the bidisperse suspensions, $\zeta_s^{eff} = (R_s^{eff}/R_s)^3 \zeta_s/(1-\phi_b)$, where ϕ_b is the volume fraction occupied by the large particles. This effective volume fraction corresponds to the volume fraction of the small particles calculated with their effective radius and their accessible volume, which is given by the total suspension volume without the volume occupied by the large particles. Based on our hypothesis, we expect deswelling of the large particles when the space between small particles is filled by the counterion clouds; this corresponds to $\zeta_s^{eff} \gtrsim 1$. By identifying the onset of deswelling in our data for $n_b = (29 \pm 3)\%$ at $\zeta = 0.67$ with the point where $\zeta_s^{eff} \approx 1$, we obtain a value of $\Delta r = (35 \pm 4)$ nm. Using this value for Δr, we can obtain the ζ corresponding to $\zeta_s^{eff} \approx 1$ for other values of n_b. For $n_b = (2.3 \pm 0.2)\%$, we obtain $\zeta \approx 0.53$, which we show with a vertical line in Fig. 1*D*. Because, in this case, $\zeta_s^{eff} > 1$ for all of the studied ζ-range, deswelling is expected throughout, consistent with our observations. In contrast, for $n_b = (79 \pm 8)\%$, the ζ-value corresponding to $\zeta_s^{eff} \approx 1$ is above any ζ used in the experiments, as shown by the vertical line in Fig. 1*F*; hence no deswelling is expected. In this case, we find that d_{nn} is comparable to that in suspensions of only large particles and significantly larger than d_{nn} in suspensions of only small particles, as shown in Fig. 1*F*, consistent with our interpretations. Note that the ζ-value associated with the onset of deswelling depends on n_b: Although the large particles are found to deswell at ζ below random close packing for $n_b = (2.3 \pm 0.2)\%$ (Fig. 1*D*), they do not deswell for any of the accessed ζ, which includes values significantly above random close packing, for $n_b = (79 \pm 8)\%$ (Fig. 1*F*). This observation suggests that a direct interaction between large and small particles is not the reason for particle deswelling.

To independently estimate Δr, we perform three Monte Carlo simulations of a single microgel particle in water with radius $R = 130$ nm, charge $-7 \cdot 10^4 e$ homogeneously distributed on the surface, and the associated counterions (*Supporting Information*). Here, e represents the elementary charge. The microgel and its counterions are confined in a spherical volume resulting in microgel volume fractions $\phi = 0.05$, 0.25, and 0.5 for the three simulations. The counterions are treated as mobile, point-like charges with radius 0.007 nm and charge e. Their distribution around the microgel particle is obtained from the simulation, as shown in Fig. S3*A*. Furthermore, the electrostatic potential, $\psi(r)$, is obtained from the sum of the potential due to the fixed surface charge and all counterions (see Fig. S3*B*). We find that most counterions are trapped close to the particle surface, where the potential energy reaches its minimum value. We find the simulation at $\phi = 0.5$ to correspond to the situation with strong overlap of the counterion clouds of neighboring particles and a higher counterion density outside than inside the particle. Following our idea of an effective particle comprising the counterion cloud and resulting in a volume fraction $\phi^{eff} \approx \phi[(R + \Delta r_{sim})/R]^3 = 1$, we obtain the estimate $\Delta r_{sim} \approx 34$ nm (*Supporting Information*), which agrees with our experimental value $\Delta r \approx 35$ nm. We further note that this value is in good agreement with what was found in a dielectric spectroscopy measurement of Δr (22).

We thus conclude that the deswelling of the large particles in the presence of smaller particles results from the osmotic pressure exerted by the bound counterions, when ζ is large enough for these ions to effectively unbind. However, this osmotic pressure difference should also be felt by the small microgels. To see whether this is the case, we perform a SANS experiment with a sample containing a majority of deuterated large particles, $n_b = (84 \pm 3)\%$, with radius $R_b = (181 \pm 4)$ nm and protonated small particles with $R_s = (137 \pm 4)$ nm (*Supporting Information*). We contrast match the deuterated large particles and probe the form factor of the small microgels in concentrated samples. Indeed, we find that the small particles deswell; from fits of the

form factors measured in the bidisperse suspension at $\zeta = 1.20 \pm 0.01$ (see Table S2) and for a dilute suspension of only small microgels, shown with diamonds and asterisks, respectively, in Fig. 4, we obtain that R_s decreases by $\Delta R_s = (42 \pm 9)$ nm. Interestingly, the effective volume fraction of the large particles, ζ_b^{eff}, in the bidisperse suspension in the experimental conditions is equal to 2.14 ± 0.03, which is larger than 1, consistent with our expectations based on the counterion-induced deswelling picture. Here, ζ_b^{eff} is computed for the large particles using the same Δr as determined above for the small microgels.

However, ΔR_s is smaller than $\Delta R_b = (63 \pm 6)$ nm for a similar ζ^{eff} (see Table S2). To understand this, recall that the swelling of the microgel not only depends on the osmotic pressure difference between the inside and the outside of the microgels, $\Delta\Pi$, but also on a sufficiently small bulk modulus, as, otherwise, the microgels would be too stiff to deswell. In fact, swelling equilibrium for the particles is achieved when the counterion-induced osmotic pressure difference is balanced by the elastic compression of the particles. Hence, swelling equilibrium is expected when $\Delta\Pi \approx K\gamma$, with the bulk modulus K and the strain γ, which we estimate as $\Delta R/R$. Considering a similar $\Delta\Pi$ for large and small microgels, we have $K_s\gamma_s = K_b\gamma_b$, and thus $\Delta R_s = K_b R_{si} \Delta R_b / (K_s R_{bi})$, where the subscripts "bi" and "si" denote the radii of the large and small microgels when fully swollen. Because $R_{si}/R_{bi} < 1$, and we also expect $K_b/K_s \lesssim 1$, we obtain that $\Delta R_s < \Delta R_b$, consistent with our observations. Note that $K_b/K_s \lesssim 1$, because both types of particles are synthesized under identical conditions but the polymerization reaction is stopped earlier for the small particles than for the large particles, implying that the cross-linker concentration has decayed less from the particle center towards the periphery for the small particles than for the large particles.

Our deswelling mechanism is also in good agreement with the deswelling of pNIPAM-based microgels reported in the literature (8, 12, 15, 24, 25). Indeed, using our estimate of Δr to obtain ζ^{eff}, the onset of particle deswelling is observed at $0.9 \lesssim \zeta^{eff} \lesssim 1.22$ in all these studies (*Supporting Information* and Table S3). We stress that we compare rather diverse systems and experiments. In some cases, particles are deuterated and protonated; in some other cases, hard and soft particles are mixed, or a majority of pNIPAM particles is mixed with a small number of large pNIPAM particles copolymerized with acrylic acid. Notably, in a recent form factor study of pNIPAM particles in crowded environments (21), deswelling was first observed at $\zeta \approx 1$, corresponding to $\zeta^{eff} = 1.8$, which is higher than our expectation. However, in this SANS experiment, the viscosimetry data show that a majority of soft deuterated particles was mixed with stiffer protonated particles with almost identical size. The softness of the two species is reversed compared to the study presented here: The behavior of the stiffer particles was followed, while the signal of the softer particles was suppressed with contrast matching. Our deswelling mechanism implies, in this case, that the bulk modulus of the protonated microgel was larger than the osmotic pressure difference set by the counterions at $\zeta^{eff} \approx 1$, thus preventing their deswelling. Furthermore, it also implies that the soft deuterated particles would experience deswelling at $\zeta < 1$, before deswelling of the stiffer protonated particles. However, the behavior of the deuterated particles was not followed in this earlier work.

In conclusion, we have unraveled the self-healing mechanism that allows bidisperse pNIPAM microgel suspensions to crystallize even at high size ratios of large and small particles (8), which would suppress crystallization if the particles were not soft (2). We find charged groups on the periphery of the particles and the corresponding clouds of bound counterions to be the key for the deswelling of the particles. At high concentrations, the counterion clouds fill the space between the particles, and, therefore, a large fraction of the bound counterions becomes effectively free to explore the volume outside the microgels. These ions establish an osmotic pressure difference between the inside and the outside of the particle, which, when larger than the microgel bulk modulus, causes particle deswelling. As pNIPAM microgels synthesized according to the same protocol become softer with increasing particle radius, large particles show a more pronounced deswelling than small particles. Furthermore, because the overlap of the counterion clouds and the associated osmotic pressure difference gradually increase in the range of concentrations around $\zeta^{eff} = 1$, the deswelling transition is not sharp but must first affect the softest part of the microgel particles, usually their soft shell. Although the model we present here captures the essential mechanism, more experiments, simulations, and theoretical work is needed to fully justify our interpretations, particularly in the ζ-regime corresponding to $\zeta^{eff} = 1$.

Remarkably, the generality of the proposed mechanism changes the role of polydispersity not only for microgel-based suspensions but, presumably, for other soft-particle suspensions. Indeed, it also at least partially explains the deswelling behavior observed with DNA-coated colloids with star-shape architecture (9). We also note that the delocalization of counterions at sufficiently large particle concentrations is reminiscent of the delocalization of electrons in a metal. However, although in the first case the behavior is classical and driven by the increase in entropy of the bound counterions when the individual microgel clouds overlap, in the second case, the effect is quantum mechanical. In both cases, however, the pressure is determined by the delocalized particles: The counterions set the suspension osmotic pressure and ultimately the osmotic pressure difference between the inside and outside of the microgel particles, causing their eventual deswelling, whereas the delocalized electrons in a metal set the pressure and hence the metal bulk modulus.

ACKNOWLEDGMENTS. The authors thank V. Trappe for fruitful discussions. Financial support from the Swiss National Science Foundation (200020_153050), the National Science Foundation, and the research partnership between Children's Healthcare of Atlanta and the Georgia Institute of Technology (4105E47) is gratefully acknowledged. SAXS data were taken on the cSAXS beamline of the Swiss Light Source, Paul Scherrer Institut, and SANS data were taken on the instruments SANS-I and SANS-II at SINQ, Paul Scherrer Institut.

1. Bragg L, Nye JF (1947) A dynamical model of a crystal structure. *Proc R Soc A* 190(1023):474–481.
2. Frenkel D (2009) Soft particles feel the squeeze. *Nature* 460(7254):465–466.
3. Gasser U (2009) Crystallization in three- and two-dimensional colloidal suspensions. *J Phys Condens Matter* 21(20):203101.
4. Bartlett P, Ottewill RH (1991) A neutron scattering study of the structure of a bimodal colloidal crystal. *J Chem Phys* 96(4):3306–3318.
5. Auer S, Frenkel D (2001) Prediction of absolute crystal-nucleation rate in hard-sphere colloids. *Nature* 409(6823):1020–1023.
6. Pelton R (2000) Temperature-sensitive aqueous microgels. *Adv Colloid Interface Sci* 85(1):1–33.
7. Fernandez-Nieves A, Fernandez-Barbero A, Vincent B, de las Nieves FJ (2000) Charge controlled swelling of microgel particles. *Macromolecules* 33(6):2114–2118.
8. Iyer ASJ, Lyon LA (2009) Self-healing colloidal crystals. *Angew Chem Int Ed* 48(25): 4562–4566.
9. Zhang J, Lettinga PM, Dhont JKG, Stiakakis E (2014) Direct visualization of conformation and dense packing of DNA-based soft colloids. *Phys Rev Lett* 113(26):268303.
10. Pelton RH, Chibante P (1986) Preparation of aqueous latices with N-Isopropylacrylamide. *Colloids Surf* 20(3):247–256.
11. Stieger M, Richtering W, Pedersen JS, Lindner P (2004) Small-angle neutron scattering study of structural changes in temperature sensitive microgel colloids. *J Chem Phys* 120(13):6197–6206.
12. Senff H, Richtering W (1999) Temperature sensitive microgel suspensions: Colloidal phase behaviour and rheology of soft spheres. *J Chem Phys* 111(4):1705–1711.
13. Lietor-Santos J-J, Sierra-Martin B, Gasser U, Fernandez-Nieves A (2011) The effect of hydrostatic pressure over the swelling of microgel particles. *Soft Matter* 7(14):6370–6374.
14. Ackerson BJ, Hayter JB, Clark NA, Cotter L (1986) Neutron scattering from charge stabilized suspensions undergoing shear. *J Chem Phys* 84(4):2344–2349.
15. Debord SB, Lyon LA (2003) Influence of particle volume fraction on packing in responsive hydrogel colloidal crystals. *J Phys Chem B* 107(13):2927–2932.
16. Brijitta J, Tata BVR, Joshi RG, Kaliyappan T (2009) Random hcp and fcc structures in thermoresponsive microgel crystals. *J Chem Phys* 131(7):074904.
17. Gasser U, Fernandez-Nieves A (2010) Crystal structure of highly concentrated, ionic microgel suspensions studied by small-angle x-ray scattering. *Phys Rev E Stat Nonlin Soft Matter Phys* 81(5 Pt 1):052401.

18. Gasser U, et al. (2013) Transient formation of bcc crystals in suspensions of poly(N-isopropylacrylamide)-based microgels. *Phys Rev E Stat Nonlin Soft Matter Phys* 88(5): 052308.
19. Loose W, Ackerson BJ (1994) Model-calculations for the analysis of scattering data from layered structures. *J Chem Phys* 101(9):7211–7220.
20. Higgins JS, Benoit HC (1994) Labelling with deuterium—How, why, and when to use. *Polymers and Neutron Scattering* (Clarendon, Oxford), pp 116–140.
21. Gasser U, et al. (2014) Form factor of pNIPAM microgels in overpacked states. *J Chem Phys* 141(3):034901.
22. Zhou J, et al. (2012) Correlation between dielectric/electric properties and cross-linking/charge density distributions of thermally sensitive spherical PNIPAM microgels. *Macromolecules* 45(15):6158–6166.
23. Pelaez-Fernandez M, Souslov A, Lyon LA, Goldbart PM, Fernandez-Nieves A (2015) Impact of single-particle compressibility on the fluid-solid phase transition for ionic microgel suspensions. *Phys Rev Lett* 114(9):098303.
24. Stieger M, Pedersen JS, Lindner P, Richtering W (2004) Are thermoresponsive microgels model systems for concentrated colloidal suspensions? A rheology and small-angle neutron scattering study. *Langmuir* 20(17):7283–7292.
25. John AN, Breedveld V, Lyon LA (2007) Phase behavior in highly concentrated assemblies of microgels with soft repulsive interaction potentials. *J Phys Chem B* 111(27):7796–7801.
26. Blackburn WH, Lyon LA (2008) Size-controlled synthesis of monodisperse core/shell nanogels. *Colloid Polym Sci* 286(5):563–569.
27. Senff H, Richtering W (2000) Influence of cross-linker density on rheological properties of temperature-sensitive microgel suspensions. *Colloid Polym Sci* 278(9):830–840.
28. Andersson M, Maunu SL (2006) Structural studies of poly(N-isopropylacrylamide) microgels: Effect of SDS surfactant concentration in the microgel synthesis. *J Polym Sci B Polym Phys* 44(23):3305–3314.
29. Heskins M, Guillet JE (1968) Solution properties of poly(N-isopropylacrylamide). *J Macromolecular Sci A Chem* 2(8):1441–1455.
30. Nicholson JW (2001) *The Chemistry of Polymers* (RSC Publ, Cambridge, UK), pp 32–33.
31. Pelton R, Hoare T (2011) Microgels and their synthesis: An introduction. *Microgel Suspensions: Fundamentals and Applications*, eds Fernandez-Nieves A, et al. (Wiley, New York), pp 3–32.
32. Ghugare SV, et al. (2011) Structural investigation on thermoresponsive PVA/Poly (methacrylate-co-N-isopropylacrylamide) microgels across the volume phase transition. *Macromolecules* 44(11):4470–4478.
33. Jones CD, Lyon LA (2000) Synthesis and characterization of multiresponsive core-shell synthesis and characterization of multiresponsive core-shell microgels. *Macromolecules* 33(22):8301–8306.
34. Amalvy JI, et al. (2004) Synthesis and characterization of novel pH-responsive microgels based on tertiary amine methacrylates. *Langmuir* 20(21):8992–8999.
35. Chen G, Imanishi Y, Ito Y (1998) pH-sensitive thin hydrogel microfabricated by photolitography. *Langmuir* 14(22):6610–6612.
36. Lietor-Santos J-J, et al. (2009) Deswelling microgel particles using hydrostatic pressure. *Macromolecules* 42(16):6225–6230.
37. Lietor-Santos J-J, Gasser U, Vavrin R, Hu ZB, Fernandez-Nieves A (2010) Structural changes of poly(N-isopropylacrylamide)-based microgels induced by hydrostatic pressure and temperature studied by small angle neutron scattering. *J Chem Phys* 133(3):034901.
38. Tanaka T (1978) Collapse of gels and the critical endpoint. *Phys Rev Lett* 40(12): 820–824.
39. Amiya T, Hirokawa Y, Hirose Y, Li Y, Tanaka T (1987) Reentrant phase transition of N-isopropylacrylamide gels in mixed solvents. *J Chem Phys* 86(4):2375–2379.
40. Destribats M, et al. (2011) Soft microgels as pickering emulsion stabilizers: Role of particle deformability. *Soft Matter* 7:7689–7698.
41. Schmidt S, et al. (2010) Adhesion and mechanical properties of pNIPAM microgel films and their potential use as switchable cell culture substrates. *Adv Funct Mater* 20(19): 3235–3243.
42. Voudouris P, Florea D, van der Schootbc P, Wyss HM (2013) Micromechanics of temperature sensitive microgels: Dip in the poisson ratio near the LCST. *Soft Matter* 9:7158–7166.
43. Zhang L, Daniels ES, Dimonie VL, Klein A (2009) Synthesis and characterization of PNIPAM/PS Core/Shell particles. *J Appl Polym Sci* 118(5):2502–2511.
44. Scotti A, et al. (2015) The CONTIN algorithm and its application to determine the size distribution of microgel suspensions. *J Chem Phys* 142(23):234905.
45. Taylor JR (1982) *An Introduction to Error Analysis* (Univ Sci Books, Herndon, VA).
46. Romeo G, Imperiali L, Kim J-W, Fernández-Nieves A, Weitz DA (2012) Origin of deswelling and dynamics of dense ionic microgel suspensions. *J Chem Phys* 136(12): 124905.
47. Ubbelohde L (1937) The principle of the suspended level. *Ind Eng Chem* 9(2):85–90.
48. Batchelor GK (1977) The effect of Brownian motion on the bulk stress in a suspension of spherical particles. *J Fluid Mech* 83(1):97–117.
49. Borrega R, Cloitre M, Betremieux I, Ernst B, Leibler L (1999) Concentration dependence of the low-shear viscosity of polyelectrolyte micro-networks: From hard spheres to soft microgels. *Europhys Lett* 47(6):729–753.
50. Bonnet-Gonnet C, Belloni L, Cabane B (1994) Osmotic pressure of latex dispersions. *Langmuir* 10(11):4012–4021.
51. Belloni L (2000) Colloidal interactions. *J Phys Condens Matter* 12(46):R549–R587.